Supplementary Materials

A mechanism for ageing in a deeply supercooled molecular glass

Authors

Andrew Cassidy,*[1] Mads R. V. Jørgensen,[2] Artur Glavic,[3] Valeria Lauter,*[4] Oksana Plekan,[5] and David Field.[1]

Affiliations

[1]A Cassidy,* D. Field, Center for Interstellar Catalysis and Department of Physics and Astronomy, Aarhus University, Ny Munkegade 120, Aarhus C, Denmark. E-mail: amc@phys.au.dk.

[2]MRV Jørgensen, Center for Materials Crystallography, iNano & Department of Chemistry, Aarhus University, Langelandsgade 140, Aarhus C, Denmark & MAX IV Laboratory, Lund University, Fotongatan 2, Lund, Sweden.

[3]A Glavic, Laboratory for Neutron Scattering and Imaging, Paul Scherrer Institut, 5232 Villigen PSI, Switzerland.

[4]V Lauter*, Neutron Scattering Division, Oak Ridge National Lab, Oak Ridge, TN 37831, USA. E-mail lauterv@ornl.gov

[5]O Plekan, Sincrotrone Trieste S.C.p.A., Area Science Park, Strada Statale 14, km 163.5, 34149 Basovizza, Trieste, Italy.

Materials and Methods

H-Methyl formate (Sigma Aldrich) and D-methyl formate (QMX laboratories) were degassed following several freze-pump-thaw cycles under vacuum conditions before use.

Surface potential measurements were performed in an UHV chamber (base pressure of 2 × 10^{-10} mbar) attached to the SGM2 beamline at the ASTRID synchrotron storage ring at Aarhus University.[1,2] Films of H-MF were prepared by background dosing techniques, on a polycrystalline gold substrate cooled with a closed-cycle He cryostat. Films were deposited with an average deposition rate of 0.48 (± 0.04) ML/s and final film thicknesses and the time taken to reach these thicknesses are provided in S. Table 1. The surface of a film was irradiated with a collimated beam of near zero-energy electrons (±1.5 meV) produced by threshold photoionization of Ar. The sample was floated, relative to ground, until the onset of current flow (2−3 fAmp) was detected by an ammeter connected to the backside of the film. The bias used to float the sample was exactly opposite in value to the potential residing at the film-vacuum interface.

A film of discrete thickness was condensed and the surface potential was measured, giving a measure of the electric field in the film. Film thickness was further increased and the surface potential was measured again, giving a new measurement of the field. Data are presented in Figure 1, as a function of time and each data point in figure 1a-c represents a surface potential measurement recorded as the film thickness was increased. Since there are no substrate or epitaxial influence on the spontelectric effect, we do not anticipate any thickness effects.[3]

S. Table 1. The final film thickness for films grown at different deposition temperatures, i.e., the final film thickness at the final point for each curve shown in figure 1 in the main text.

Td / K	**Final film thickness / ML**	**Time at final thickness / s**	**Td / K**	**Final film thickness / ML**	**Time at final thickness / s**	**Td / K**	**Final film thickness / ML**	**Time at final thickness / s**
40	760	10016	**57**	1124	10606	**77.5**	920	16096
45	945	10634	**60**	645	9910	**80**	920	19080
50	1070	12550	**63**	1130	10932	**83**	1720	13276
55	740	12330	**65**	650	11952	**85**	1810	11000
	-		**70**	1020	11888	**86.5**	2820	14984
	-		**75**	714	7780	**88**	2685	16050
	-			-		**89**	2460	12030
	-			-		**90.5**	1430	11872

Polarised Neutron reflectivity (PNR) measurements were made at the Magnetism Reflectometer instrument at the Spallation Neutron Source at Oak Ridge National Laboratory.[4] Magnetically-contrasted neutron scattering was used to measure the self-diffusion of molecules of MF on molecular length scales as a function of sample temperature. A 10 mm x 20 mm Si (100) substrate was sonicated in propanol and acetone each for 10 minutes and then adhered to an Inconel substrate holder with silver paste. An electron beam evaporator (Modified Varian 3118 with a four-pocket e-beam gun, a 6kW electron beam power supply (MDC e-Vap CVS-6)) was used to produce a Co/Pt bilayer on top of the Si with 3 nm of each metal. This composite substrate was mounted on a closed cycle liquid helium cryostat, allowing for cooling down to 20 K. High vacuum conditions were maintained with a base pressure of approximately 1×10^{-7} mbar. Composite films of MF (H-MF) and fully deuterated MF (D-MF, in which all H atoms are replaced with D), were prepared *in situ*, on top of the magnetically labelled substrate, following a method described elsewhere.[5] Vapours were deposited from a gas line with a base pressure below 1×10^{-6} mbar. A standard needle valve was used to expose the cooled substrate to a controlled background pressure of the desired isotopically substituted material. The rate of deposition was 0.1 Å/s. A highly collimated neutron beam was incident on the sample under a grazing angle Θ and the scattered neutrons were registered by a 2D neutron detector as a function of time-of-flight and scattering angle. Choppers constrain the total bandwidth of the neutron beam incident on the sample to ∼3 Å when operating at 60 Hz. The experiments were performed with neutron wavelength bands of 2.9−5.9 Å and 5.1−8.1 Å. The time-of-flight directly correlates to the neutron wavelength, λ, and thus the scattering vector, or wave vector transfer Q perpendicular to the sample surface, is defined as $Q=4\pi \sin\Theta/\lambda$. Neutron reflectometry probes the depth profile of the scattering length density (SLD) of the film; The SLD is determined by the distribution of atoms per unit volume in each layer and is equivalent to SLD = $\Sigma^{i}_{n} N_i b_i$, where N_i is the number density of the i^{th} component, and b_i is the coherent scattering length of the i^{th} component, in the system. The scattering length *b* is a constant tabulated for most nuclei, and isotopes of the same element can have different *b*. In particular, it is negative for hydrogen (H) ($b = -3.742e^{-5}$ A) and positive for deuterium (D) ($b = 6.74e^{-5}$ A), thus providing a very high contrast for element sensitivity in neutron scattering experiment.[6] One of the strengths of this technique is its ability to measure thicknesses of layers with a very high precision of around 0.5 nm. Scattering data quantify depth-sensitive changes to the microscopic structure of the film, via the primary structural relaxation mechanism, that is, molecular diffusion, with at least two orders of magnitude increased sensitivity above that achieved in similar experiments.[7,8]

For each reflectivity, five measurements were performed using different wavelength bands and Θ angles to cover a q range from <0.01 $Å^{-1}$ to 0.16 $Å^{-1}$ with 2% relative resolution $\Delta q/q$. Modelling of the neutron reflection data was performed using the standard Parratt recursion formalism[9] implemented in the GenX software.[10] The number of free parameters was reduced by defining the layer geometry only for the initial deposition and then evolving the H/D-diffusion numerically using 100 slices within the layer. In this way the layer boundaries are accurately described and only one diffusion constant, D, for each temperature is added as a free parameter. Small variations, on the Å scale, of the total thickness were observed. These were attributed to adsorption and desorption of residual gas. Final refinement of all model parameters was performed on the full set of measured data for any one sample, to avoid biasing the structural results. The substrate part of the model was first refined with a reflectivity measurement before film growth and subsequently held constant.

Supplementary neutron scattering data

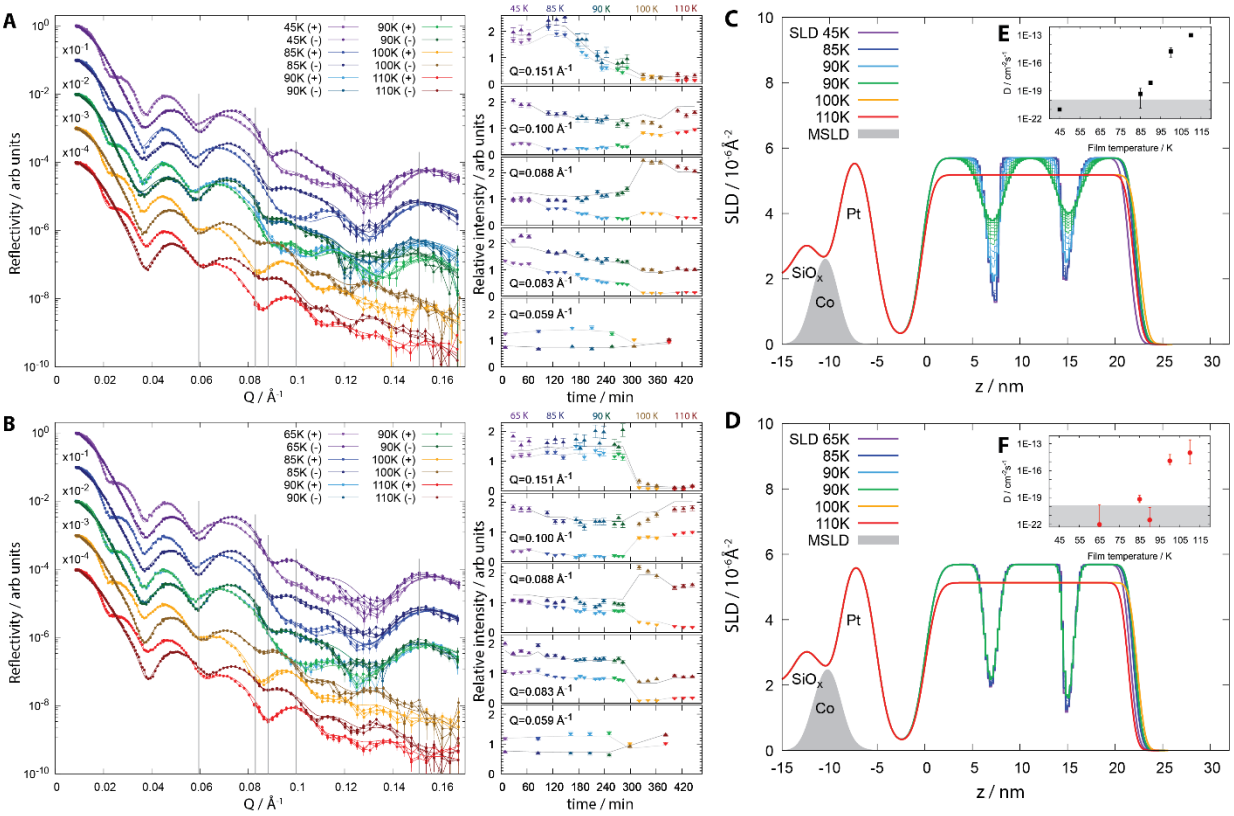

S. Figure 1. Neutron scattering data from two distinct penta-layered films of methyl formate. Top – data for a film with Td=45 K; bottom – data for a film with Td=65 K. **A-B LHS** Reflectivity plots, as a function of scattering vector magnitude Q, for a film prepared at **A** Td=45 K and **B** Td=65 K, and gradually annealed to higher temperatures. Magnetic contrast variation allows for two data curves, labelled + and -, to be recorded at each temperature. Raw data are shown as points with fits shown as overlying lines. **RHS** Relative intensity, resulting from fits at specific Q values, was extracted and plotted as a function of time, where 0 min indicates the beginning of the first measurement. There are several time values for each annealing temperature (see main text) and colour has been used to distinguish between annealing points. Errors arise from signal to noise variation. Lines represent fits resulting from the self-diffusion model. **C-D** Scattering length density profiles, **C** Td=45 K and **D** Td=65 K, and then annealed to gradually higher temperatures. Colour is used to distinguish between annealing steps but fits allow for several SLDs to be constructed at each temperature. **E-F** Self-diffusion coefficients, D, are plotted as a function of film temperature and then annealed to progressively higher temperatures. The grey area indicates the lower limit of detection and diffusion coefficient values in this regime are too low to be modelled reliably.

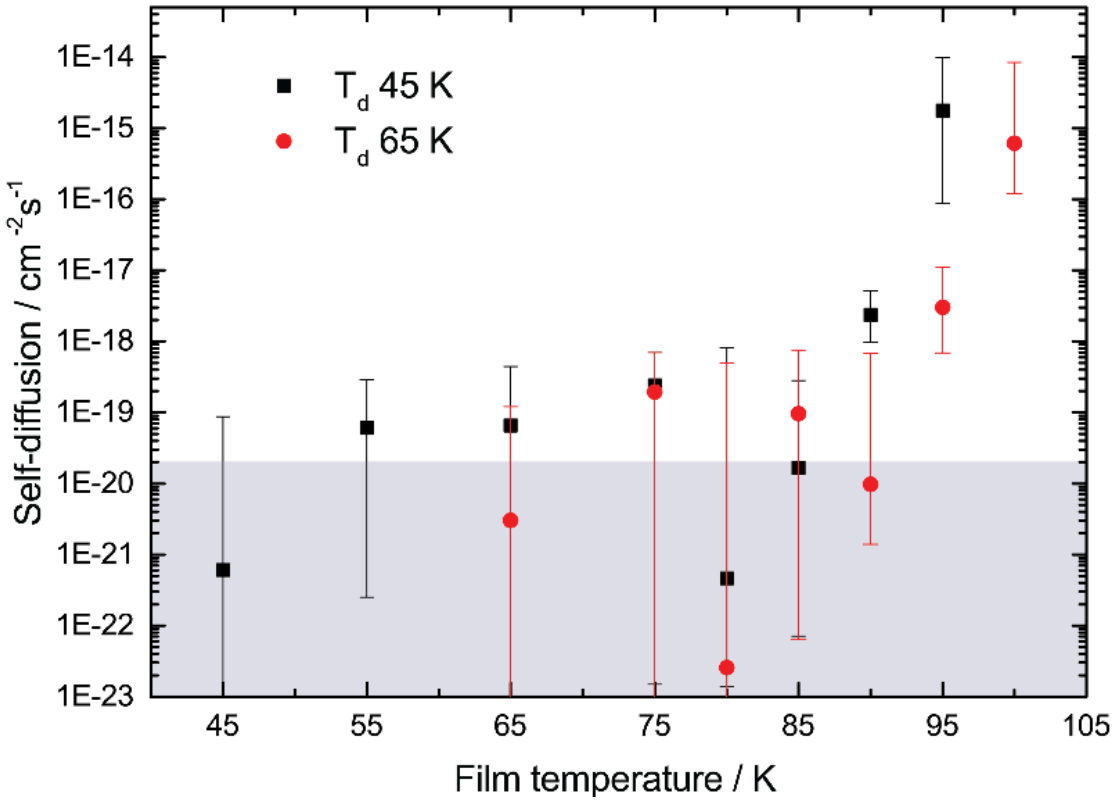

S. Figure 2. Self-diffusion coefficients, D, are plotted as a function of film temperature for two distinct tri-layered films of methyl formate prepared at Td=45 K and Td=65 K, and then annealed to progressively higher temperatures. The grey area indicates the lower limit of detection and diffusion values in this regime are too low to be modelled reliably. From Td until ≥ 90 K, both the Td=45 K and Td=65 K demonstrate very low self-diffusion values, on the threshold of what can be reliably measured using this technique. From 90 K upwards the self-diffusion values begin to rise in a coherent manner. This dataset was used to determine the annealing steps for the penta-layered films. The self-diffusion values remain negligible at 85 K and so penta-layered films were annealed from Td to this temperature, as a first annealing step.

Supplementary x-ray diffraction data

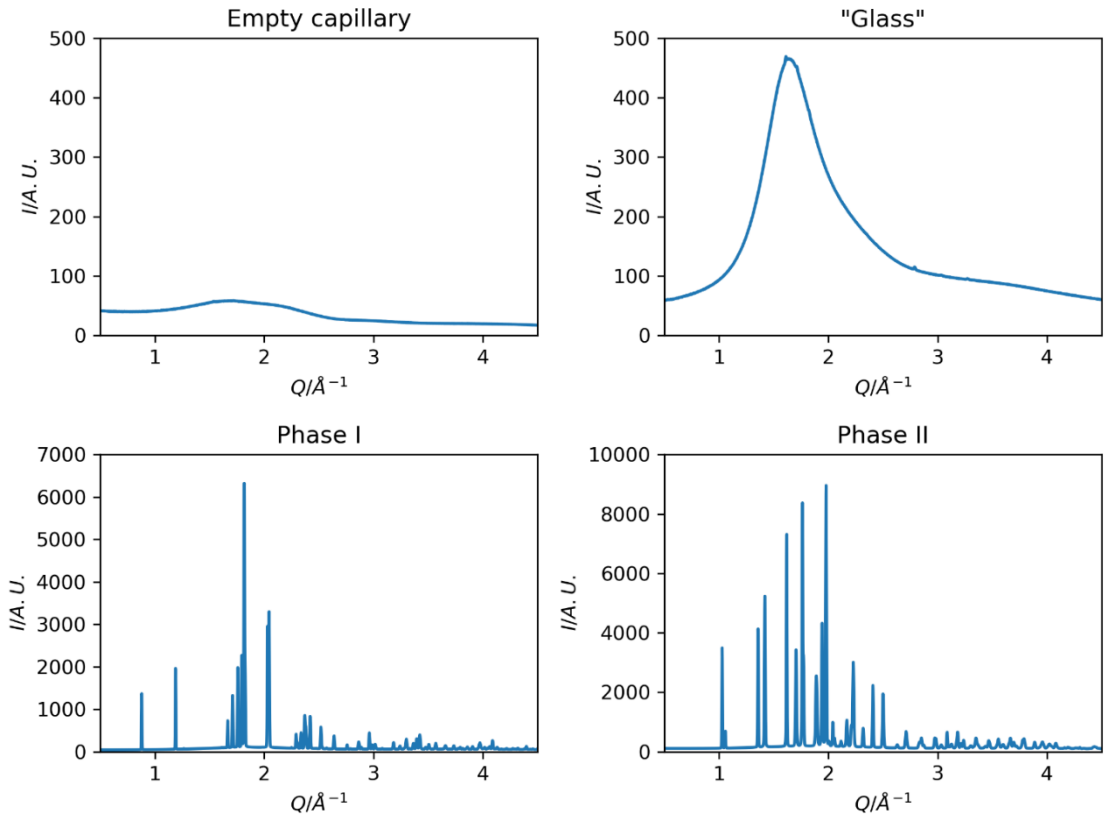

S. Figure 3. X-ray scattering data from methyl mormate collected at 87 K. Top left: Glassy state, top right: Empty capillary, bottom left: Phase I, bottom right: Phase II.

Synchrotron X-ray scattering/diffraction data was measured at the BioMAX beamline at MAX IV Laboratory using a wavelength of 0.918 Å and an Dectris Eiger 16 M detector.[11] A NIST LaB_6 (SRM660c) standard was used to determine the detector position and wavelength. The azimuthal integration of the raw 2D images was performed using the software tool Dioptas 0.4.1.[12]

A glass capillary with an inside diameter of 500 µm and a wall thickness of 10 µm was cut to length and mounted in a magnetic sample holder. The tip was dipped into the methyl formate liquid at room temperature and a small amount of liquid was drawn into the capillary due to surface tension.

The sample was mounted on the goniometer in a vertical orientation with the tip pointing down. As the capillary was open in both ends this (presumably combined with evaporation at the open tip) lead to visible motion in the upper sample meniscus. Data was collected using 720 degree oscillations to improve the powder statistics and minimize effects of preferred order in the crystalline states.

The sample was cooled using an open flow liquid nitrogen cryostream set to 87 K. 87 K was the lowest temperature possible with this particular device. The temperature was measured in the nozzle, and thus it is likely that the sample temperature was slightly higher than the quoted temperature. The cryostream was pre-cooled and could be moved to the sample position in less than a second using a pneumatic actuator. Upon moving the cryostream to the sample position the movement of the liquid meniscus was immediately arrested, however the sample remained as clear

as in the liquid state. X-ray scattering from the sample only contains broad features confirming that the sample is in a glassy state, see the top left panel of S.figure 2. In the scattering pattern there are a few very weak peaks on top of the amorphous signal. These weak features are presumably ice formation on the outside of the capillary. To confirm that this is indeed methyl formate we also collected scattering data on an empty capillary, see the top right panel of S.Figure 2.

While investigating the homogeneity of the sample, the sample was suddenly observed to turn opaque and began to yield sharp diffraction peaks, indicating a phase transformation to crystalline. This behaviour was reproducible over several heating and cooling cycles. Two distinct powder diffraction patterns, here called Phase I and Phase II, were present in the samples. In most instances data were obtained from mixtures of the two, but in some locations the sample was nearly phase pure (either phase I or II) as shown in the lower panels in S. Figure 2.

Indexing of Phase I

An automatic peak search was performed in WinPLOTR (Version Sept. 2018[13]); and these were subsequently used for indexing in the program DICVOL04.[14] The routine yielded two potential, and similar, monoclinic solutions. Both solutions were used for profile matching in the Fullprof program (Version 6.30[15]). One solution gave slightly better agreement factors and was thus selected as the most probable unit cell. The fit of the profile matching is shown in S. figure 3. The unit cell has the following parameters: a=17.5052(2) Å, b=6.63187(5) Å, c=13.2857(2) Å, ß=107.716(1) °, volume = 1469.23(1) $Å^3$ and symmetry p2/m. Assuming that the density of the solid is identical to the liquid this implies that there are 14.4 molecules per unit cell. The density is likely higher at lower temperature and combined with the inversion symmetry it is likely that there are 16 molecules in the unit cell leading equaling a density of 1.09 g/cm^3.

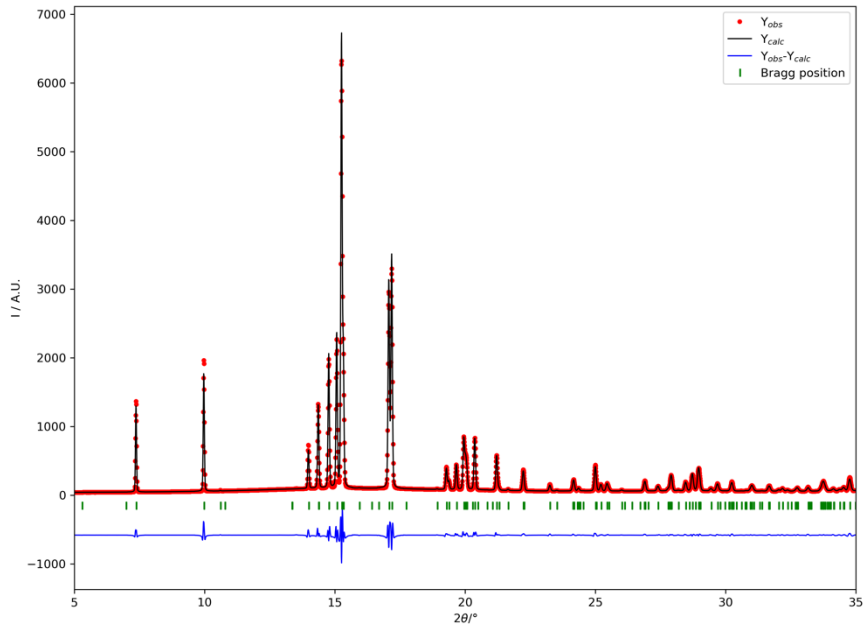

S Figure 4. Profile fit of phase I.

Indexing of Phase II

Indexing of phase II was attempted in the same way as described for phase I above, however, the indexing routine could not find a solution able to index all peaks, suggesting that multiple phases

are present. Further attempts using two cells were not able to index all peaks satisfactorily, suggesting that at least three crystalline phases were present. No further attempts have been pursued in order to index these phases.

Supplementary surface potential measurements during sample anneal

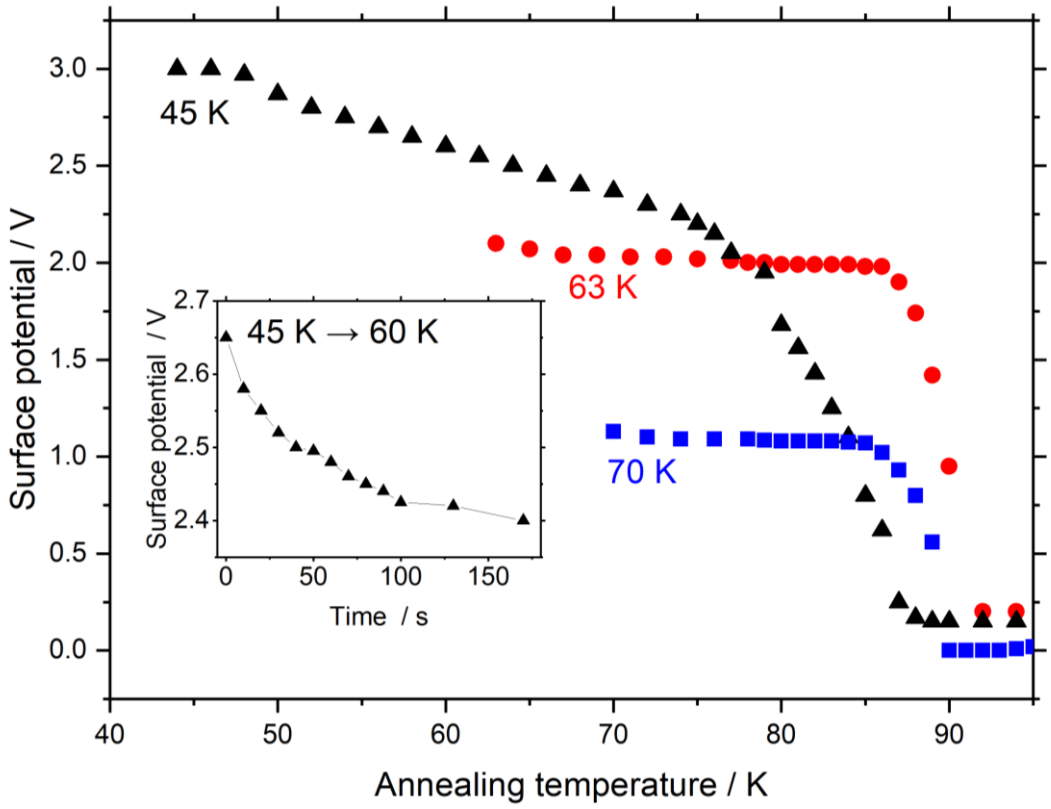

S Figure 5. Surface potential measurements, recorded at the film-vacuum interface, for layers of methyl formate as a function of annealing temperature. Data for films with different deposition temperatures (Td) are shown as different colour traces; Td 45 K, Td 63 K and Td 70 K. The inset shows data for a film with Td45 K subsequently annealed to 60 K, with data shown as a function of time. All films were of the same nominal thickness, 1175 ML (± 20 %), where prepared with the same deposition rate, 0.48 (± 0.04) ML/s and were heated at the same rate, 3 min/K. Temperature errors are less than 0.5 K and surface potentials were measured to within 1 mV.

A film prepared at 45 K, with an initial surface potential of 3.0 V, demonstrates strong temperature dependence in surface potential, with the surface potential decreasing consistently as the temperature is increased. The inset demonstrates the variation of the surface potential for a film with Td 45 K, subsequently annealed to 60 K. The surface potential drops by 0.4 V over 3 hours. Films prepared at 65 K and 75 K harbour less potential to begin with but show almost no variance in surface potential with time or as the annealing temperature is increased, until a sudden decay at 90 K. By 90 K all films show negligible surface potential. Figure 1 (main text) demonstrates that films of methyl formate can have different physical properties, depending on the temperature at which the film is grown. That the same film thickness of methyl formate produces a lower surface potential when deposited at 65 K, compared to 45 K, is known, and expected, based on analysis using the spontelectric model.[1] The surface potential, in all cases, turns to 0 V as the temperature approaches 90 K because the material passes through a glass transition point where translational molecular movements, beyond single molecular length scales, become allowed on laboratory

timescales. Films prepared with Td ≤ 55 K behave differently upon anneal because these films are less stable upon deposition, with stability decreasing as Td is decreased.

Calculating Activation Energies

Lag periods were measured from the data presented in **Fig 1** in the main text. The lag period is defined as the time taken before the first molecules begin to rotate away from a dipole-oriented conformation. The inverse lag time can be used to establish a rate for this rotation process. The degree of dipole orientation is defined as $<\mu_z>/\mu$, where $<\mu_z>$ indicates the component of the molecular dipole, μ, pointing in the direction of the electric field, that is, normal to the plane of the film. The process of the decay of $<\mu_z>/\mu$ has been modelled as first order and the corresponding rate coefficients and activation energies are shown in columns 2&3 of **Table 1** in the main text.

From the rate coefficients, we calculate the effective activation energies E^*_{lag}. For this purpose we require values of pre-exponential factors, A, in $k^{1st} = A.exp - \left(E^*_{lag}/kT\right)$. Errors on values of E^*_{lag} are dominated by the uncertainty in *A*. Values of E^*_{lag} vary by ~10% between $A = 5 \times 10^{10}\ s^{-1}$ and $5 \times 10^{12}\ s^{-1}$, where the former value has been adopted as more appropriate to a system driven by rotational motion. The corresponding values of E^*_{lag} are shown in **Table 1** of the main text. The activation barrier is the energy barrier to overcome molecular locking for each film separately, *i.e.*, each film, with its distinct Td, is treated as a unique system and we use the lag times, also collected at Td, to estimate the barrier for each system separately.

Acknowledgements

Fabrication of the substrates for neutron reflectivity measurements was conducted by Alexandra C Steffen at the Center for Nanophase Materials Sciences, which is a DOE Office of Science User Facility. This research used resources at the Spallation Neutron Source, a DOE Office of Science User Facility operated by the Oak Ridge National Laboratory. We highly appreciate the support of H. Ambaye during the preparation of the equipment for the NR experiments. We are grateful to the MAX IV Laboratory for beam time at the BioMAX beamline. We highly appreciate the support of Dr. Mirko Milas, Dr. Uwe Mueller, and Dr. Innokenty Kantor during these synchrotron experiments. We acknowledge MAX IV Laboratory for time on Beamline BioMAX under Proposal 20190134. Research conducted at MAX IV, a Swedish national user facility, is supported by the Swedish Research council under contract 2018-07152, the Swedish Governmental Agency for Innovation Systems under contract 2018-04969, and Formas under contract 2019-02496.

Bibliography

1 O. Plekan, A. Cassidy, R. Balog, N. C. Jones and D. Field, *Physical chemistry chemical physics : PCCP*, 2012, **14**, 9972–6.
2 R. Balog, P. Cicman, N. C. Jones and D. Field, *Phys. Rev. Lett.*, 2009, **102**, 073003.
3 A. Cassidy, O. Plekan, R. Balog, J. Dunger, D. Field and N. C. Jones, *J. Phys. Chem. A*, 2014, **118**, 6615–6621.
4 V. Lauter, H. Ambaye, R. Goyette, W. T. Hal Lee and A. Parizzi, *Physica B*, 2009, **404**, 2543–2546.
5 A. Cassidy, M. R. V. Jørgensen, A. Rosu-Finsen, J. Lasne, J. H. Jørgensen, A. Glavic, V. Lauter, B. B. Iversen, M. R. S. McCoustra and D. Field, *The Journal of Physical Chemistry C*, 2016, **120**, 24130–24136.
6 Neutron Activation and Scattering Calculator, https://www.ncnr.nist.gov/resources/activation/, (accessed May 6, 2020).
7 M. K. Mapes, S. F. Swallen and M. D. Ediger, *J. Phys. Chem. B*, 2006, **110**, 507–511.

8 S. F. Swallen, M. K. Mapes, Y. S. Kim, R. J. McMahon, M. D. Ediger and S. Satija, *Journal of Chemical Physics*, , DOI:10.1063/1.2191492.
9 L. G. Parratt, *Physical Review*, 1954, **95**, 359–369.
10 M. Björck and G. Andersson, *Journal of Applied Crystallography*, 2007, **40**, 1174–1178.
11 T. Ursby, K. Åhnberg, R. Appio, O. Aurelius, A. Barczyk, A. Bartalesi, M. Bjelčić, F. Bolmsten, Y. Cerenius, R. B. Doak, M. Eguiraun, T. Eriksson, R. J. Friel, I. Gorgisyan, A. Gross, V. Haghighat, F. Hennies, E. Jagudin, B. Norsk Jensen, T. Jeppsson, M. Kloos, J. Lidon-Simon, G. M. A. de Lima, R. Lizatovic, M. Lundin, A. Milan-Otero, M. Milas, J. Nan, A. Nardella, A. Rosborg, A. Shilova, R. L. Shoeman, F. Siewert, P. Sondhauss, V. O. Talibov, H. Tarawneh, J. Thånell, M. Thunnissen, J. Unge, C. Ward, A. Gonzalez and U. Mueller, *J Synchrotron Rad*, 2020, **27**, 1415–1429.
12 C. Prescher and V. B. Prakapenka, *High Pressure Research*, 2015, **35**, 223–230.
13 T. Roisnel, J. Rodriguez-Carvajal, R. Delhez and E. J. Mittenmeijer, in *WinPLOTR: a Windows tool for powderdiffraction patterns analysis materials science forum*, 2000, pp. 20–23.
14 A. Boultif and D. Louër, *Journal of Applied Crystallography*, 2004, **37**, 724–731.
15 J. Rodríguez-Carvajal, *Physica B: Physics of Condensed Matter*, 1993, **192**, 55–69.